Check for updates

Comparative photocatalytic activity of sol–gel derived rare earth metal (La, Nd, Sm and Dy)-doped ZnO photocatalysts for degradation of dyes†

Umair Alam, [ID] [a] Azam Khan,[a] Danish Ali,[a] Detlef Bahnemann [ID] [bc] and M. Muneer*[a]

Rare earth metal doping into semiconductor oxides is considered to be an effective approach to enhance photocatalytic activity due to its ability to retard the electron–hole pair recombination upon excitation. Herein, we report the synthesis of different rare earth metal (La, Nd, Sm and Dy)-doped ZnO nanoparticles using a facile sol–gel route followed by evaluation of their photocatalytic activity by studying the degradation of methylene blue (MB) and Rhodamine B (RhB) under UV-light irradiation. Different standard analytical techniques were employed to investigate the microscopic structure and physiochemical properties of the prepared samples. The formation of the hexagonal wurtzite structure of ZnO was established by XRD and TEM analyses. In addition, the incorporation of rare earth metal into ZnO is confirmed by the shift of XRD planes towards lower theta values. All metal doped ZnO showed improved photocatalytic activity toward the degradation of MB, of which, Nd-doped ZnO showed the best activity with 98% degradation efficiency. In addition, mineralization of the dye was also observed, indicating 68% TOC removal in 180 min with Nd-doped ZnO nanoparticles. The influence of different operational parameters on the photodegradation of MB was also investigated and discussed in detail. Additionally, a possible photocatalytic mechanism for degradation of MB over Nd-doped ZnO nanoparticles has been proposed and involvement of hydroxyl radicals as reactive species is elucidated by radical trapping experiments.

1. Introduction

Dyes and pigments are considered as the major class of industrial organic pollutants because they are toxic and carcinogenic in nature. In addition, the removal of these water-borne pollutants is difficult due to the non-biodegradable components present in them.[1–3] The conventional wastewater treatment applied for the degradation of these pollutants led to the transfer of one form of pollutant to another form, which are more toxic than that of the parent molecule.[4–6] Taking into account of the above problems, there is a need to develop a method that could significantly degrade the pollutants present in wastewater. In this regard, the use of semiconductor based advanced oxidation processes (AOPs) has achieved significant acceptance owing to their potential applicability to mineralize organic pollutants in aqueous suspensions.[7–9] Over the years, a variety of semiconducting materials have

ᵃDepartment of Chemistry, Aligarh Muslim University, Aligarh-202002, India. E-mail: readermuneer@gmail.com; m.muneer.ch@amu.ac.in

ᵇPhotocatalysis and Nanotechnology, Institut fuer Technische Chemie, Gottfried Wilhelm Leibniz Universitaet Hannover, Callinstrasse 3, D-30167 Hannover, Germany

ᶜPhotoactive nanocomposite materials, Saint-Petersburg State University, Ulyanovskaya Str, Peterhof, Saint-Petersburg, 198504, Russia

† Electronic supplementary information (ESI) available. See DOI: 10.1039/c8ra01638k

been employed for the abatement of toxic organic pollutants under UV or visible light irradiation.[10–17] Among these, ZnO and TiO$_2$ stand out as the most promising materials due to their non-toxic and stable nature.[8,10,18–24] Earlier reports indicate that ZnO has the ability to sufficiently mineralize the organic pollutants into less toxic substances and can absorb more quanta of light than that of the TiO$_2$.[25–28] The above merits make ZnO a better candidate for the degradation of organic compounds under light irradiation. However, the major obstacle that impedes the efficacy of ZnO is the quick recombination of charge carrier which makes it an ineffective photocatalyst during photocatalytic degradation process.[29–31] It is well established that the surface charge transfer and intrinsic charge carrier recombination are correlated with the structure and optical properties of photocatalysts. Keeping these issues in mind, semiconductive oxides should be modified in such a way that the separation efficiency of photogenerated charge carriers could be increased to ameliorate the photocatalytic performance.

Tremendous efforts have been devoted to prevent the recombination rate of charge carriers by metal doping and construction of heterojunction between two semiconductors.[29–34] One of most appealing issue is the doping of metal ions into ZnO nanoparticles which are known to enhance the photocatalytic activity by inhibiting charge carriers recombination.[33] In particular, rare earth metals are gaining increasing interest as an alternative dopant of

other metals to modify photocatalysts for the degradation of organic pollutants.[34–36] Previous studies indicate that the interaction of rare earth metals with semiconductors could enhance the photocatalytic performance as their ability to form complexes with Lewis bases by the interaction of functional groups with f-orbital of rare earth metals.[37,38] Thus, it is speculated that the incorporation of rare earth metals could concentrate the dye substrates onto the surface of semiconductor thereby enhancing the photocatalytic activity.[39] Furthermore, rare earth metals have been a centre of interest in the domain of photocatalysis as their ability to trap the photogenerated electrons, which can effectively eliminate the charge carrier recombination during the photocatalytic reaction. For instance, Vaiano et al. has modified the ZnO with praseodymium and found the excellent photocatalytic activity under both UV and visible light irradiation.[31] Okte reported the synthesis of different Ln^{3+} (La, Eu, Gd, Dy and Ho)-loaded ZnO and tested their roles on the decolorization of methyl orange under various conditions.[35] Complementary to the reported findings, the role of rare earth metals doping into ZnO would be of interest for the research community working in the field of photocatalysis primarily for the elimination of waste water.

To the best of author's knowledge, very few studies have been carried out on the comparison of photocatalytic activity of different rare earth metal-doped ZnO photocatalysts for the elimination of organic pollutants.[36,40] Although there are reports on the comparative photocatalytic study of rare earth metals doped ZnO nanoparticles, but the reaction mechanism of photocatalysis has not yet been well explored using dye as model pollutant. Inspired by the trailblazing studies reported by Vaiano et al.[31] and Okte,[35] we have made an attempt to develop a sol–gel route for the synthesis of rare earth metals (RE = La, Nd, Sm and Dy) doped ZnO nanoparticles. The potential applicability of RE-doped ZnO nanoparticles was assessed by studying the decomposition of dye derivative under different operational conditions and a possible photocatalytic mechanism of MB degradation has been discussed and elucidated by the reactive species determination results.

2. Experimental details

2.1. Materials

Zinc acetate dihydrate and rare earth metal nitrates were purchased from Sigma-Aldrich. The water used in all experiments was double distilled. Methylene Blue (MB) and Rhodamine B (RhB) were selected as model organic pollutants. The different scavengers such as disodium ethylenediaminetetraacetate (EDTA-2Na), 1,4-benzoquinone (BQ) and isopropyl alcohol (IPA) used in this study were purchased from Alfa-Aesar. Nitric acid and sodium hydroxide were obtained from S.D. fine chemicals. Commercial ZnO was purchased from Merck-India. All the chemical used in this study were of analytical grade and were used without any further purification.

2.2. Preparation of rare earth metal (RE)-doped ZnO

The different RE (La, Nd, Sm and Dy)-doped ZnO nanoparticles were prepared by a facile sol–gel method using zinc acetate and rare earth metal nitrate as the corresponding precursor. A schematic diagram showing the synthesis of RE-metal doped ZnO nanoparticles is shown in Fig. 1. For each RE-doped ZnO nanoparticles, 5 g of zinc acetate dihydrate was dissolved in 20 mL of water containing the metal nitrates (RE^{3+} = 1 at%) and stirred vigorously for 30 min to get a homogenous suspension, and then heated at 80 °C for 1 h with vigorous stirring. After complete dissolution of above mixture, a freshly prepared 1 M aqueous NaOH solution was added dropwise to maintain the pH 11. The above solution was allowed to hydrolyze at room temperature to get a gel product. The obtained product was filtered and washed several times with water followed by ethanol to remove the impurities. The product was dried overnight at 100 °C and then calcined at 500 °C for 6 h to obtain different rare earth metal doped ZnO nanoparticles. Pure ZnO was prepared under analogous conditions as mentioned above except the addition of dopants.

2.3. Material characterization

The crystallinity of the prepared samples was characterized by X-ray diffraction (XRD, Shimadzu 6100) in the range of 20–80 (2θ) with (Cu Kα radiation (1.54065 Å)) operated at a voltage of 30 kV and current of 15 mA. SEM images of pure and Nd-doped ZnO were recorded on JSM-6510 microscope (JEOL) scanning electron microscope. Transmission electron microscopy (TEM) images were obtained on a JEOL-JEM 2100 instrument operating at 120 keV. The optical properties of the prepared catalysts were determined by UV-Vis diffuse reflectance spectra (Perkin Elmer Lambda 35 UV-Vis spectrophotometer) using $BaSO_4$ as a standard reference material. Photoluminescence spectra were
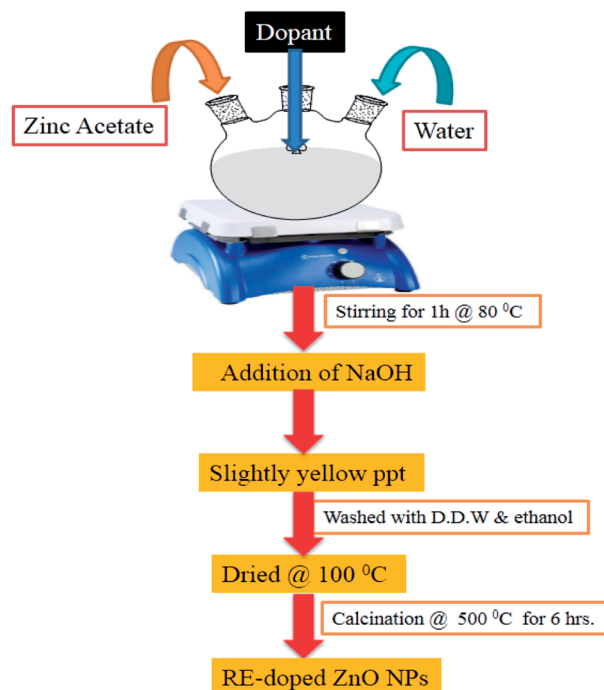

Fig. 1 Schematic diagram of preparation of RE-metal doped ZnO nanoparticles.

recorded using Hitachi (F-2500) spectrofluorimeter with an excitation wavelength 320 nm at room temperature. Thermogravimetric analysis (TGA) analysis was carried out to investigate the thermal stability of the prepared samples by Shimadzu 60H over the temp range of 20–700 °C with heating ramp rate 10 °C min^{-1}. The specific surface areas and pore size structures of prepared samples were determined by using Quantachrome Autosorb I Automated Gas Sorption System Instruments.

2.4. Photocatalytic experiments

The synthesized materials were tested for the decomposition of MB and RhB under UV-light irradiation in an immersion well photochemical reactor made of Pyrex glass, which is equipped with a magnetic stirring bar, a water circulating jacket and an opening to supply air. UV-light was provided by 125 W medium pressure mercury lamp (Philips), which is vertically placed inside the photochemical reactor. The light intensity was measured using a UV light intensity detector (Lutron UV-340) and was found in the range between 1.49–1.51 mW cm^{-2}. The reaction pH was adjusted by adding required amount of dilute aqueous HNO$_3$ or NaOH solution before irradiation. In all photocatalytic experiments, the desired amount of photocatalyst was suspended in 180 mL of aqueous solution of dye (10 ppm) and then the suspension was sonicated for 5 min followed by stirring the solution for 15 min under dark condition to attain the adsorption–desorption equilibrium before the suspension was exposed to UV-light source. The samples (5 mL) were withdrawn at different time intervals, centrifuged and analyzed spectrophotometrically by monitoring the change in absorbance at λ_{max} = 663 nm for MB and λ_{max} = 553 nm for RhB. The degradation efficiency of catalyst was estimated by the following expression:

$$\text{Degradation efficiency} = (C_0 - C_t)/C_0 \times 100\% \quad (1)$$

where C_0 is the initial concentration of MB or RhB and C_t is the concentration at different time intervals on irradiation by UV-light. The extent of mineralization of dye was also determined by measuring the decrease in TOC content as a function of irradiation time using Shimadzu TOC-V$_{CSH}$ analyzer. During TOC measurements, higher concentration of dye and catalyst were used keeping all other photochemical conditions similar as mentioned above.

To assess the role of reactive species involved in the degradation of MB, different scavengers such as IPA, BQ and EDTA-2Na were added to detect the hydroxyl radical ($^\bullet$OH), superoxide radical (O$_2$$^{\bullet-}$) and hole (h$^+$), respectively. For this experiment, 3 mM concentration of scavenger and 2 g L^{-1} loading content of Nd-doped ZnO nanoparticles were added to MB solution (180 mL, 10 ppm) and the solution was irradiated under analogous conditions as mentioned in photocatalytic test.

In addition, the generation of hydroxyl radical formed during photocatalytic experiment of terephthalic acid solution in the presence of Nd-doped ZnO photocatalyst was evaluated using fluorescence technique with excitation wavelength fixed at 315 nm. The PL signal obtained at 425 nm is directly related to the formation of fluorescence adduct i.e. 2-hydroxyterephtahlic acid.

3. Results and discussion

3.1. Structural and morphological analysis

The crystal phase and structure of the prepared samples were analyzed by X-ray diffraction analysis. The XRD patterns of pure and RE-metal doped ZnO nanoparticles are shown in Fig. 2a. The peaks observed in pure as well as in rare earth metal-doped ZnO nanoparticles are in accordance with the standard sample of the hexagonal ZnO as reported earlier (JCPDS-36-1451).[35] No other peaks corresponding to dopants and impurities are detected, indicating that the samples are in highly crystalline and pure form. The XRD patterns of all RE-doped ZnO showed a shift towards lower theta value compared to the standard ZnO nanoparticles due to the incorporation of RE-metals into ZnO. In order to see the effect of doping of RE metals on diffraction peaks, magnified range of XRD patterns (2θ = 30–38) are
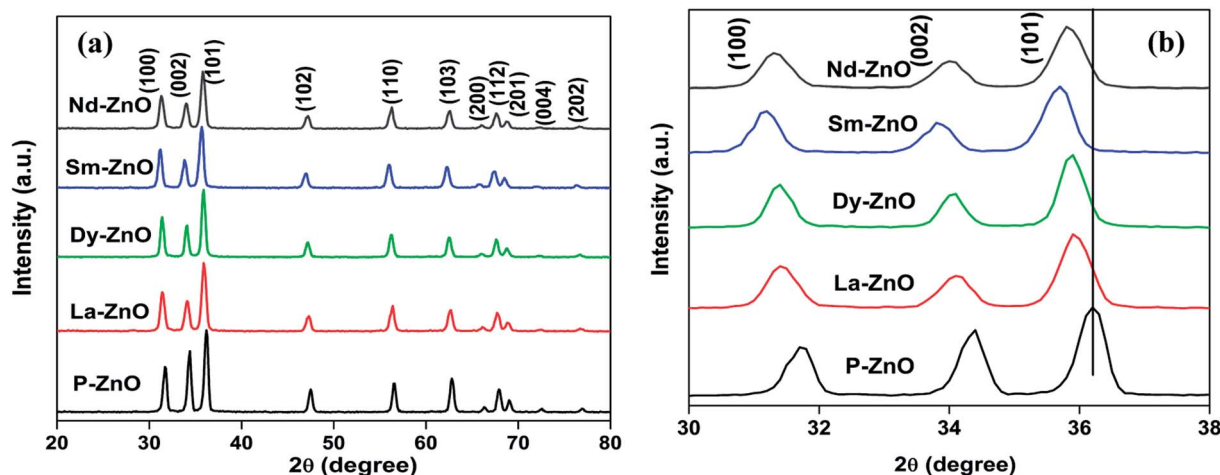

Fig. 2 (a) XRD patterns of P-ZnO, La-ZnO, Dy-ZnO, Sm-ZnO and Nd-ZnO nanoparticles and (b) magnified (30−38) XRD patterns.

presented in Fig. 2b. The shift of diffraction peak towards lower theta value may be due to the expansion of unit cell because of mismatch of ionic radii. Furthermore, the shift also gives an evidence of incorporation of metals into ZnO. Similar results are reported in the literature where metals cause the analogous changes in the crystal structure.[31,40,41] Moreover, introduction of RE-metals into ZnO causes broadening and less intense peak, implying inhibition in crystal growth.[42] The diffraction pattern of Nd-doped ZnO nanoparticles are weaker than that of other rare earth metal doped samples, implying profound effect of Nd-doping on the reduction of crystallinity of ZnO nanoparticles. Due to the large ionic radii of the rare earth metals, it is difficult to substitute Zn from its lattice and therefore, the most suited place of rare earth metals ions is to stay in the grain boundary.[43] The crystalline size of the prepared samples were calculated by using Scherrer formula as given in eqn (2).

$$D = K\lambda/\beta \cos \theta \qquad (2)$$

where D is the crystallite size of the nanoparticles, K is the shape factor, λ is the wavelength of the radiation used, β is full width at half maxima (FWHM) in radians and θ is the diffraction angle. The average crystallite size of the prepared samples were estimated by the full width at half maxima (FWHM) of the XRD peak (101) using Debye–Scherer equation and the results are given in Table 1. The crystallite size of the samples were found in the range of 17.1–12.3 nm with an error limit of ±1 nm.

The morphology of pure and Nd-doped ZnO nanoparticles was examined by SEM analysis and the results are shown in Fig. 3. Nearly spherical shape with irregular size of nanoparticles could be seen for pure ZnO as indicated in Fig. 3a and b. After the incorporation of Nd onto ZnO nanoparticles the surface becomes rough, manifesting the dispersion of Nd on ZnO nanoparticles as shown in Fig. 3c. The modification of ZnO with Nd maintains the uniformity of the nanoparticles. Such changes on the surfaces of ZnO are considered as the available adsorption sites for the dye molecule on the surface of ZnO nanoparticles. Fig. 3c also shows a highly dispersed aggregate, which could be advantageous for photocatalysis because they do not only assist to adsorb organic pollutants on the surface of photocatalysts but also help in the penetration of light during illumination. To further confirm the incorporation of Nd into ZnO nanoparticles, EDS analysis for Nd-doped ZnO nanoparticles was carried out, as shown in Fig. 3d. The results clearly indicate that Nd-doped ZnO nanoparticle contains three elements such as Nd, Zn and O, suggesting the existence of Nd into ZnO nanoparticles.

The surface morphology and particle size of undoped and Nd-doped ZnO nanoparticles were further investigated by TEM analysis and the images are shown in Fig. 4. From TEM images (Fig. 4a and b) of pure ZnO nanoparticles, it is clear that the morphology of pure ZnO nanoparticles is hexagonal as well as spherical in shape without agglomeration. The particle size of the pure ZnO nanoparticles was found to vary in the range between 15–30 nm, which is in agreement with average crystallite size of pure ZnO nanoparticles calculated by the Scherrer formula. The structure of ZnO nanoparticles remains same after modification with Nd into ZnO. The only difference is the coverage of nanoparticles with a layer of neodymium particles as shown in Fig. 4c. The lattice fringe with inter-planar distance of 0.26 nm corresponds to the plane of (101) of ZnO nanoparticles as shown in Fig. 4d. The particle size obtained from the TEM results are almost consistent with crystallite size obtained from the XRD analysis.

3.2. UV-Vis diffuse reflectance spectra (UV-Vis DRS)

The influence of RE-metal doping on optical properties of ZnO nanoparticle was examined by UV-Vis DRS analysis. Fig. 5a shows the UV-Vis absorption spectra of pure ZnO (P-ZnO) and different RE-metal doped ZnO nanoparticles. It could be seen from the figure that the absorption edge at 381 nm in pure ZnO is mainly due to electronic transition from VB to CB, which is in accordance with previous report.[44] While all RE-metals doped ZnO nanoparticles exhibit absorption shift towards higher wavelength, manifesting the incorporation of metals into ZnO which may be due to the formation of impurity state between VB and CB of ZnO. The absorption shift towards the higher wavelength of the prepared samples are found in the following order; Dy-ZnO > Nd-ZnO > Sm-ZnO > La-ZnO. The shift in the absorption edge could be attributed to the charge-transfer transition between the f electrons of rare earth metal ions and conduction or valence band of ZnO as reported earlier.[45] The optical bandgap energies of the prepared samples were calculated from the well-known Tauc equation and the plots are shown in Fig. 5b.[8] The calculated bandgap energies of the samples were found in the range between 3.25–3.17 eV as mentioned in Table 1. The results given in Table 1 reveal that the absorption of metal-doped and pure ZnO lie in the UV-region and therefore all irradiation experiments were carried out using UV-light source.

3.3. Photoluminescence (PL) study

PL spectroscopic study is widely used to investigate the fate of photogenerated electron–hole pair recombination on irradiated semiconducting materials.[46] It is well-known that the PL intensity is directly related to recombination rate of electron–hole pair. Generally, weaker PL response leads to slow recombination rate thereby increasing the life-time of photogenerated charge carries and hence better photocatalytic activity.[47] Fig. 6 shows the PL spectra at excitation wavelength of 320 nm for pure and RE-doped ZnO nanoparticles. It could be seen from

Table 1 The shift in peak (101) position, crystallite sizes and bandgap energy of pure and different RE-metals doped ZnO nanoparticles

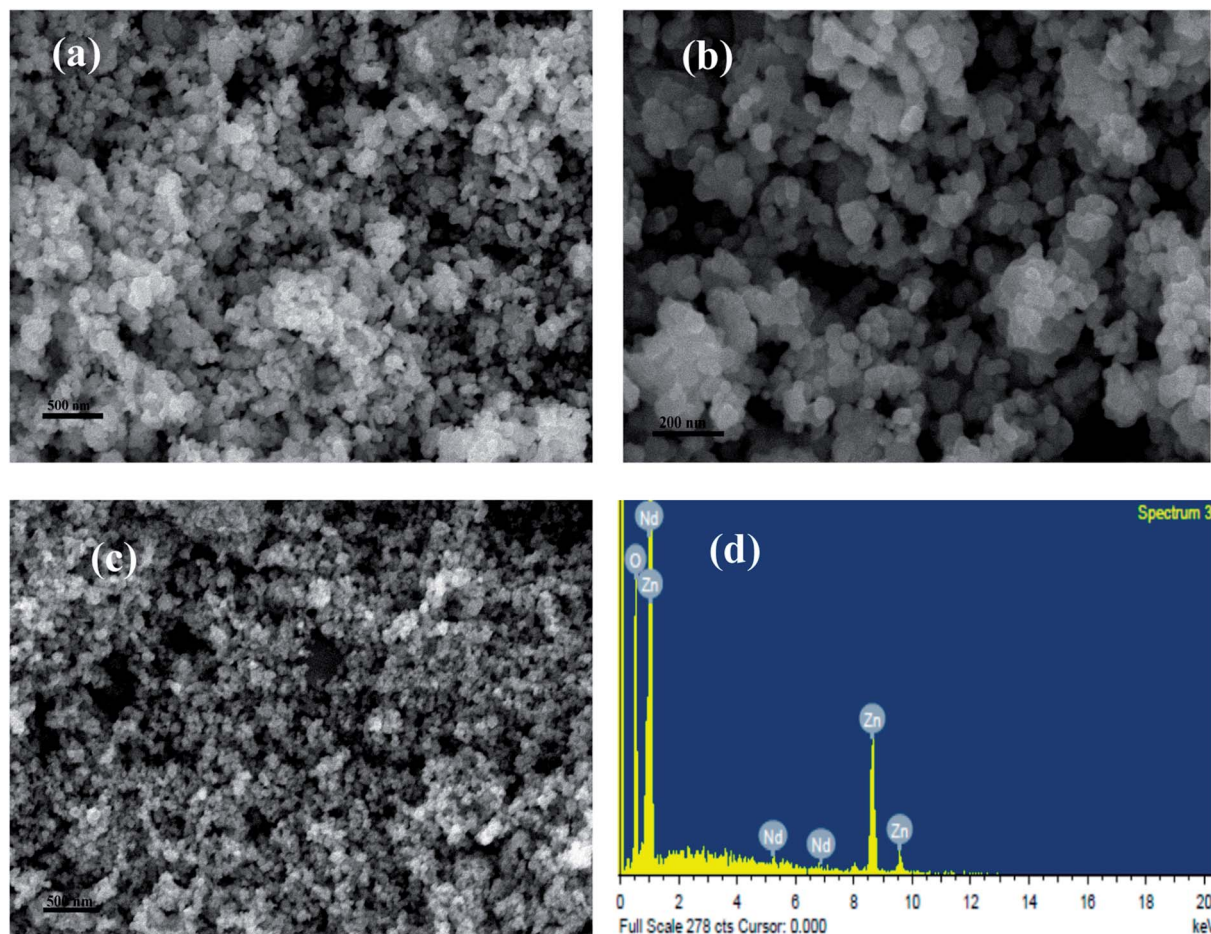| Catalyst	Peak (101) position at 2θ degree	Crystallite size (nm)	Bandgap (eV)
P-ZnO	36.205	17.10 ± 1	3.25
La-ZnO	35.936	15.45 ± 1	3.23
Dy-ZnO	35.870	14.73 ± 1	3.17
Sm-ZnO	35.691	13.68 ± 1	3.19
Nd-ZnO	35.825	12.31 ± 1	3.18

Fig. 3 SEM images of (a and b) P–ZnO, (c) SEM image of Nd–ZnO and (d) EDS spectra of Nd–ZnO.

the figure that the PL spectra of all RE-doped ZnO are comparatively lower than that of the pure ZnO nanoparticles. The results clearly indicate that the electron–hole pair recombination could be minimized by rare earth metals doping, leading to better separation of photo-generated charge carriers, which can ultimately benefit the photocatalytic activity of the materials. As compared to pure and other RE-doped ZnO nanoparticles, Nd-doped ZnO nanoparticles showed significant quenching in the PL emission signal suggesting Nd doping may lead to better separation efficiency and hence better photocatalytic activity.

3.4. TGA analysis

The effect of temperature on Nd-doped ZnO nanoparticles was evaluated by thermogravimetric analysis. Both pure and Nd-doped ZnO nanoparticles were gradually heated from 20 to 700 °C and the weight loss as a function of temperature is shown in Fig. S1.† It could be seen from the figure that slight weight loss in both materials were observed up to 400 °C, which may be due to the loss of water molecule adsorbed on the surface of ZnO nanoparticles.[48] The samples show high stability even after incorporation of Nd into ZnO. No significant weight loss was observed after 400 °C, indicating exceptionally high

thermal stability of the prepared samples. In contrast to pure ZnO, Nd-doped ZnO nanoparticles shows relatively more weight loss due to more adsorption of water molecule on the surface of Nd-doped ZnO nanoparticles. The above results confirm that most of the unwanted materials were decomposed during calcination at 500 °C to achieve pure crystalline products.

3.5. BET surface area analysis

The surface area is an important factor that may contribute to enhance the photocatalytic activity because it can provide more active sites to adsorb pollutants on the surface of catalyst. The surface area and the pore size of pure and Nd-doped ZnO nanoparticles were determined by N_2 adsorption–desorption isotherms and their results are shown in Fig. 7 and Table 2. The adsorption/desorption isotherms exhibit a classical type-IV nitrogen isotherm with a hysteresis loop.[46] The calculated surface area of pure and Nd-doped ZnO nanoparticles were found to be 30.31 and 140.9 m^2 g^{-1}, respectively. The relative pore volume of pure ZnO is measured to be 0.027 cm^3 g^{-1}, which is found to be lower than that of Nd-doped ZnO (0.148 cm^3 g^{-1}) nanoparticles. The results demonstrate that the doping with Nd could increase the surface area of ZnO nanoparticles. The higher surface area may facilitate
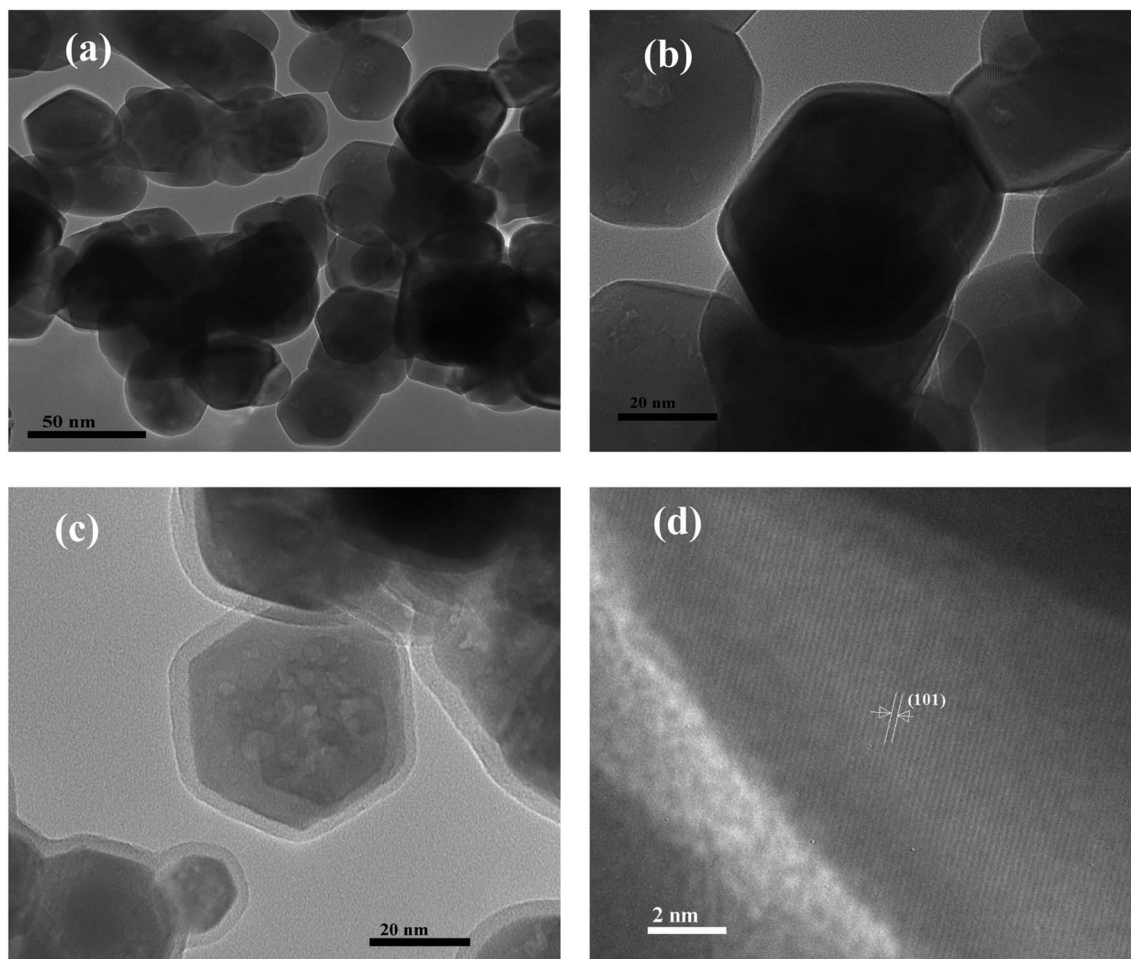
Fig. 4 TEM images of (a and b) P-ZnO, (c) Nd-ZnO and (d) HRTEM image of Nd-ZnO.

the adsorption of organic pollutants on the surface of catalyst, which in turn, enhances the photocatalytic activity. Therefore, Nd-doped ZnO nanoparticles is anticipated to have better photocatalytic performance than undoped ZnO nanoparticles.

3.6. Photocatalytic activity

Methylene blue has been considered as a virulent organic pollutant which poses a major threat to the environment because of its widespread use in the industrial production.
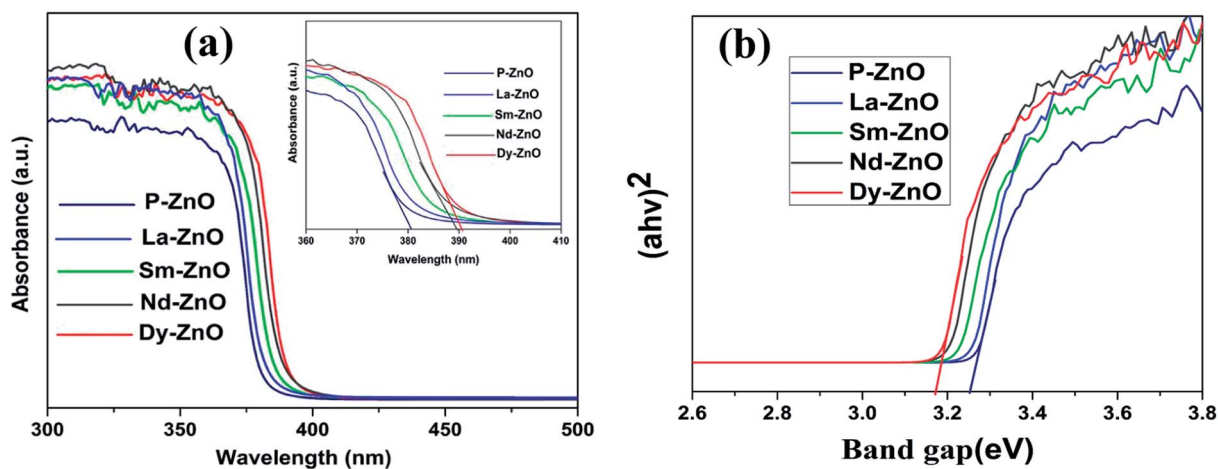

Fig. 5 (a) UV-Vis diffuse reflectance spectra of P-ZnO, La-ZnO, Sm-ZnO, Nd-ZnO and Dy-ZnO, magnified absorption spectra (inset) and representative Tauc plots (b).
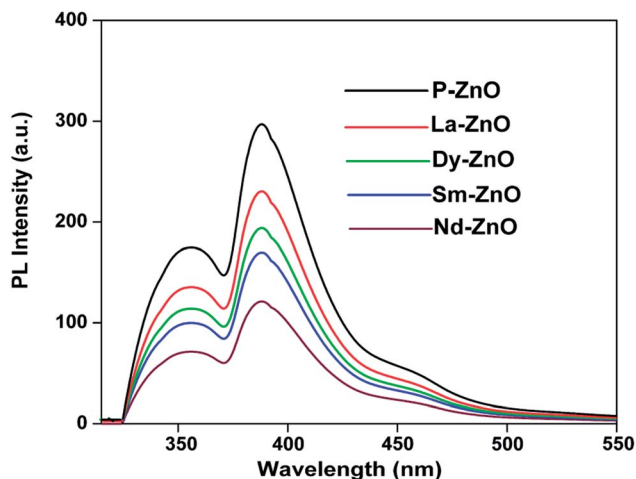
Fig. 6 PL spectra of P-ZnO, La-ZnO, Dy-ZnO, Sm-ZnO and Nd-ZnO at excitation wavelength of 320 nm.

Thus, in this study, we have chosen MB as a target organic pollutant to appraise the photocatalytic efficiency of the prepared pure and rare earth metal doped ZnO under UV-light irradiation. The characteristic absorption peak of MB at 663 nm was chosen to monitor the photocatalytic efficiency of the prepared samples *via* spectrophotometrically. Fig. 8a shows the change in absorption intensity at different time intervals on irradiation of an aqueous solution of MB in the presence of Nd-doped ZnO nanoparticles, whereas Fig. 8b shows the change in concentration of MB as a function of time in the presence of pure and different rare earth metal doped samples. It is pertinent to mention here that the decrease in absorption intensity centered at 663 nm is due to loss of chromophoric groups responsible for its color as mentioned in earlier studies as well.[49,50] It is evident from the figure that all rare earth metal doped ZnO showed enhanced photocatalytic activity toward the degradation of MB compared to pure ZnO. The activity trend for different rare earth metal doped ZnO for degradation of MB lies in the order: Nd-ZnO > Sm-ZnO > Dy-ZnO > La-ZnO, respectively, showing highest activity for Nd-doped ZnO. Control

experiments were carried out in the absence of catalyst under analogous conditions, where no significant loss of MB was observed. The photocatalytic activity results shown in Fig. 8b indicate that pure ZnO affords 52.4 ± 4% degradation, while all modified ZnO photocatalysts with similar doping content (1 at%) showed commendable photocatalytic activity under analogous conditions. Furthermore, the photocatalytic performance of the prepared samples was compared with commercial ZnO under the analogous conditions. The commercial ZnO (C-ZnO) showed the lower activity than that of the prepared samples and could only degrade 38% of dye within 25 min of irradiation time.

We have further compared the photocatalytic activity of prepared samples more accurately and quantitatively by studying the degradation kinetics of MB. The degradation curve showing the change in concentration *vs.* irradiation time for photocatalytic degradation of MB shown in Fig. 8b could be fitted reasonably well by an exponential decay curve suggesting pseudo-first-order kinetics. Fig. 9 shows the linear regression curve fit of the natural logarithm for the concentration of MB at different irradiation time. For each experiment, the degradation rate constant of MB was determined using eqn (3).

$$-\ln(C_t/C_0) = kt \qquad (3)$$

where C_0 and C_t are initial and final concentrations at fixed irradiation time and k is the pseudo-first order rate constant. The calculated rate constants for different samples for degradation of MB are mentioned in Table S1.† It is evident from the table that the rate constant obtained for doped samples were higher than that of pure ZnO nanoparticles and are in accordance with activity trend as mentioned before with highest value for Nd-doped ZnO nanoparticles.

To test the effectiveness of the prepared catalysts, we have performed the photocatalytic test on another cationic dye *i.e.* Rhodamine B (RhB) under UV light irradiation. The change in absorption spectra of RhB centered at 553 nm in the presence of Nd-doped ZnO nanoparticles is shown in Fig. S2a.† The photocatalytic performance of the prepared samples was compared
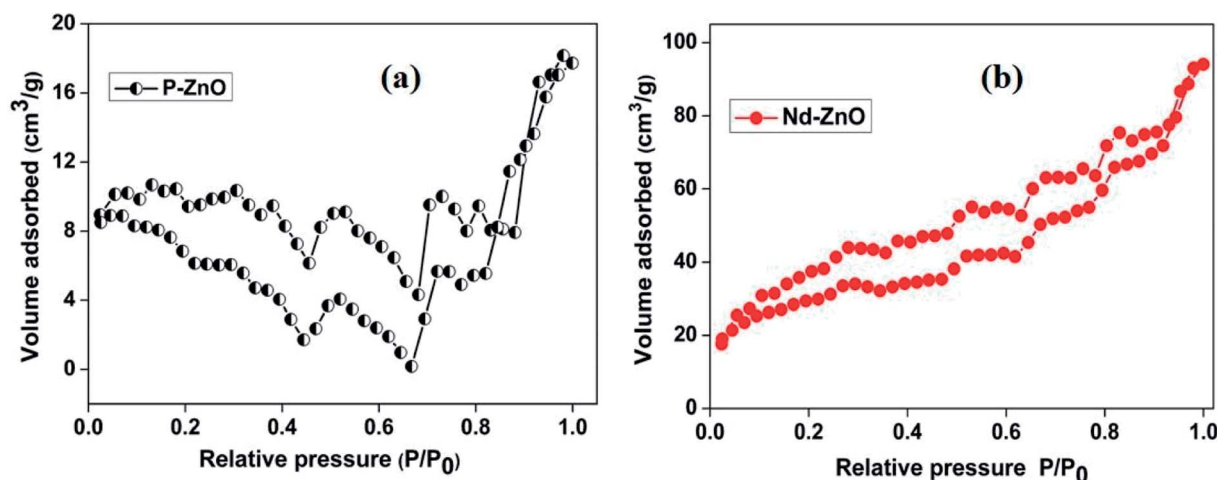

Fig. 7 N$_2$ adsorption−desorption isotherm of pure (a) and Nd-doped ZnO (b).

Table 2 Textural properties of pure and Nd-doped ZnO nanoparticles

Sample	S_{BET} ($m^2\ g^{-1}$)	Average pore diameter (Å)	Pore volume ($cm^3\ g^{-1}$)
P-ZnO	30.31	36.25	0.027
Nd-ZnO	140.9	41.39	0.148

by monitoring the change in concentration of RhB as a function of irradiation time in the presence of different catalysts. For this dye as well, Nd-doped ZnO was found to show the excellent photocatalytic performance than that of the other catalysts and commercial ZnO as shown in Fig. S2b.† The photocatalytic activity trend for different doped samples has been found to be similar to that observed in the case of MB.

The efficiency of Nd-doped ZnO was also established by measuring the depletion in TOC content of MB as a function of irradiation time. Fig. S3† shows the mineralization of MB measured in terms of TOC% removal on irradiation of an aqueous solution of MB (50, 100 ppm) in the presence of Nd-doped ZnO (4 g L^{-1}). The results indicate the 64–68 ± 6% mineralization of MB in 180 min of irradiation. The result further suggests that Nd-doped ZnO nanoparticles not only decolorizes MB but also mineralizes it into innocuous substances. All further operational parameters such as catalyst loading, effect of reaction pH were conducted with pure and Nd-doped ZnO nanoparticles.

3.6.1. Effect of pH on degradation of MB. The pH of the reaction mixture in heterogeneous photocatalysis plays a significant role because it dictates the surface charge properties of the catalysts and adsorption behavior of the pollutants on the surface of catalysts.[51–54] The effect of pH on degradation of MB in the presence of Nd-ZnO was studied in the pH range of 5–11. The pH of the reaction mixture was adjusted at the start of the irradiation and not maintained throughout the course of the reaction. Fig. S4† shows MB percent degradation at different pH values in the presence of Nd-ZnO. It could be seen from the

figure that degradation efficiency increases with increasing pH and highest degradation is observed at pH 10. A further increase in pH may lead to decrease in the photocatalytic activity. The better activity under alkaline pH could be explained on the basis of electrostatic attraction between the negative charged catalyst and positive charged MB, which facilitate the adsorption of MB on the surface of catalyst. The point of zero charge of metal doped ZnO nanoparticles is reported to be 9.0 ± 0.3.[42,55] The reason for the reduction in photocatalytic activity at low pH is due to slight dissolution of ZnO nanoparticles as ZnO on reaction with acid could produce corresponding salts at low pH value.[56,57] Higher degradation rate of different cationic dyes in basic medium has also been reported by several authors using modified ZnO nanoparticles.[58–61] In addition, the effect of pH on degradation of MB is also tested with pure ZnO nanoparticles and the results and discussion are given in ESI.†

3.6.2. Effect of catalyst dosage on degradation of MB. In order to evaluate the effect of catalyst dosage on photodegradation of MB, we have performed the experiment by varying the catalyst loading from 1 to 3 g L^{-1} while other conditions remain unchanged as conducted in photocatalytic activity. Fig. S5† shows MB percent degradation as a function of catalyst loading where degradation efficiency increases with increasing catalyst dosage from 1 to 2 g L^{-1} and then decreases. The increase in photodegradation efficiency at 2 g L^{-1} could be attributed to the availability of more active sites and penetration of light, which could ultimately enhance the photocatalytic activity. The inhibition in photocatalytic activity at 3 g L^{-1} is an increase in the turbidity of the solution and aggregation of nanoparticles, which could cause decrease in penetration of light and reduce the active sites of the catalyst.[62,63] Additionally, the effect of catalyst dosage of pure ZnO nanoparticles on degradation of MB is investigated and its results are provided in ESI.†

3.6.3. Effect of initial MB concentration. The initial pollutant concentration is an important parameter from application point of view. The effect of initial (MB) concentration was
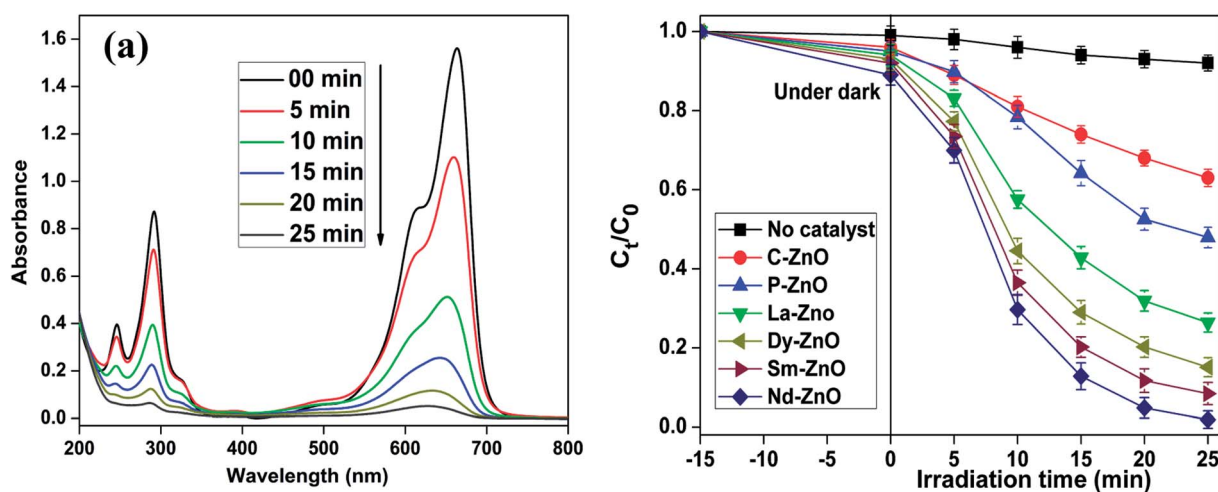

Fig. 8 Decrease in absorption spectra of MB at different time intervals in the presence of Nd-ZnO (a) and change in concentration of MB calculated by following the decrease in λ_{max} at 663 nm in the presence of different samples under UV-light irradiation (b); catalyst used 2 g L^{-1}, pH = 10. Error bars showing the standard deviation of three experiments repeated under analogous conditions.
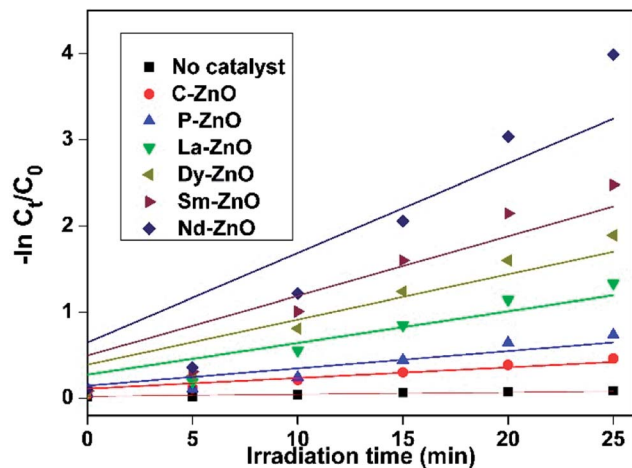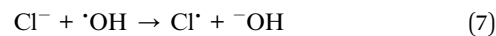
Fig. 9 Kinetic study of MB degradation in the presence of pure and doped ZnO nanoparticles.

studied by varying concentration of MB from 10–30 ppm in the presence of Nd-doped ZnO nanoparticles with catalyst loading of 2 g L^{-1} at pH 10 with UV light irradiation under analogous conditions. The result of MB degradation at varying substrate concentrations is shown in Fig. S6.† The results indicate that the % degradation of MB decreases with increase in initial concentration from 10 ppm onwards. The reason for the slow degradation of MB at higher concentration is due to intense color of the dye which does not allow the light to fall on the catalyst to generate charge species.[55,57] The amount of formation of reactive species by the catalyst is the same while increasing the initial concentration of substrate and therefore, limited reactive species against high concentration of substrate leads to decrease in photocatalytic activity.

3.6.4. **Effect of oxidants on degradation of MB.** The addition of oxidants such as $(NH_4)_2S_2O_8$, $KBrO_3$ and H_2O_2 have been proven to enhance the photodegradation of organic pollutants as these oxidants could reduce the recombination rate of charge carriers by accepting electron during photocatalysis.[64,65] The effect of oxidants on the degradation of MB was studied at fixed concentration of $(NH_4)_2S_2O_8$, $KBrO_3$ (2 mM) and H_2O_2 (10 mM), respectively. The catalyst dosage and concentration of MB were same as used in catalytic activity. The effect of all additives on degradation of MB in the presence of Nd-doped ZnO nanoparticles is shown in Fig. S7.† As expected, all the oxidants promoted the degradation and dye was found to decolorize within 15 min of illumination. The increase in photocatalytic activity in the presence of additives is probably due to the formation of other oxidizing species that might help to degrade the MB effectively.[65] The most profound effect was observed in the case of H_2O_2. This could be explained on the basis of the fact that addition of H_2O_2 increases the concentration of ˙OH, thereby improving the rate of photocatalytic oxidation. The enhancement in photocatalytic activity on addition of oxidant is likely due to the effective separation of charge carriers and generation of oxidizing species.

3.6.5. **Effect of inorganic anions on degradation of MB.** It is well known that inorganic anions such as sulphate and chloride are frequently present in water systems[66] and therefore the effect of these anions (NaCl and Na_2SO_4) on the degradation of MB with Nd-doped ZnO nanoparticles was investigated and the results are shown in Fig. S8.† In this study, photocatalytic experiments were carried out using MB (10 ppm), Nd-doped ZnO (2 g L^{-1}), anions such as NaCl and Na_2SO_4 (0.2 mM) under analogous conditions. It could be seen from the figure that all anions make an adverse effect on the degradation of pollutant under investigation with significant reduction with Cl$^-$ ions. The reduction in photocatalytic could be explained on the basis of the fact that the anions get adsorbed on the surface of catalysts thereby the adsorption of MB molecules on the catalysts surface gets restricted. The anions may block the active sites thereby reducing the availability of attack of ˙OH radicals and decreasing the photocatalytic activity. The inhibitory effect of anions which act as scavengers are summarized in eqn (4)–(7).

$$SO_4^{2-} + h^+ \rightarrow SO_4^{\cdot-} \tag{4}$$

$$SO_4^{2-} + {}^\cdot OH \rightarrow SO_4^{\cdot-} + {}^-OH \tag{5}$$

$$Cl^- + h^+ \rightarrow Cl^\cdot \tag{6}$$

$$Cl^- + {}^\cdot OH \rightarrow Cl^\cdot + {}^-OH \tag{7}$$

3.6.6. **Reusability of the catalyst.** The long-term stability of the catalysts is also an important factor from application point of view to mitigate the organic pollutants from waste water. In this experiment, the stability was evaluated by reusing the photocatalysts (pure and doped ZnO) for five consecutive cycles for the degradation of an aqueous solution of MB. Before applying for next cycle, the catalysts were thoroughly washed with water followed by ethanol to remove the impurities and then dried at 100 °C for 4 h. No significant loss in the photocatalytic efficiency was observed in the case of RE-doped ZnO nanoparticles after five successive runs, as depicted in Fig. S9.† The results imply that RE-doped ZnO nanoparticles could be an excellent photocatalyst for the degradation of MB with good stability. In comparison to RE-doped ZnO nanoparticles, pure ZnO nanoparticles shows a significant loss in photocatalytic activity under the analogous conditions. The reduction in photocatalytic activity of pure ZnO nanoparticles may be due to the photocorrosion of ZnO, which arises due to quick recombination of charge carriers. The results confirm that the doping with suitable metals could improve the stability of the catalysts. Furthermore, RE metals could act as a good acceptor and capture the photogenerated electron from ZnO under UV-light irradiation by preventing ZnO from photocorrosion.[67]

3.6.7. **Trapping studies and photocatalytic mechanism.** A series of radical trapping experiments have been employed to ascertain the main reactive species involved in the degradation of MB using Nd-ZnO nanoparticles. For this experiment, different scavengers such as isopropyl alcohol (IPA),

benzoquinone (BQ) and disodium ethylenediaminetetraacetate (EDTA-2Na) have been used to trap HO$^{•}$, O$_2^{•-}$ and holes formed during the photo-oxidation process.[68,69] Fig. 10 shows percent degradation of MB in the presence of different scavengers using Nd-ZnO on irradiation of an aqueous solution of MB for 25 min under analogous conditions. The figure clearly indicates that scavenger-free photocatalytic system exhibits maximum % decomposition rate compared to scavenger-assisted system. The results also indicate that the addition of IPA showed significant reduction in MB degradation by quenching hydroxyl radical formed in the reaction mixture indicating this species being actively involved in the degradation process. Moreover, the photodegradation of MB is slightly reduced on addition of BQ and EDTA-2Na, which give further indication of involvement of hydroxyl radical as the main reactive species as BQ not only traps photogenerated electron but also minimizes the possibility of double electron reduction, whereas, EDTA-2Na traps the hole during reaction process.

In addition, the sole contribution of hydroxyl radicals was further confirmed by terephthalic acid as a probe molecule using PL analysis technique. It has been reported earlier that terephthalic acid readily reacts with hydroxyl radical (formed during semiconductor mediated photoinduced process) to give a fluorescent product *i.e.* 2-hydroxyterephthalic acid (TA-OH), which could be monitored by PL analysis to assess the involvement of hydroxyl radical in the reaction medium. Fig. 11 shows the change in PL intensity of TA-OH under UV-light irradiation of a basic solution of terephthalic acid for 25 min in the presence of Nd-doped ZnO nanoparticles. It could be seen from the figure that the PL intensity (due to the formation of hydroxyl radical) gradually increases with increasing irradiation time as evidenced by PL signal observed at 425 nm. The aforementioned results suggest that hydroxyl radical is the major reactive species involved in the degradation of MB in the presence of Nd-ZnO nanoparticle under our reaction condition.

On the basis of abovementioned results and reported literature, a possible photocatalytic mechanism for the

Fig. 11 Hydroxyl radical trapping PL spectral changes at different time intervals over Nd-ZnO in a basic solution of terephthalic acid.

degradation of MB over Nd-doped ZnO nanoparticles under UV-light irradiation is proposed and illustrated in Fig. 12. The bandgap energy of Nd-doped ZnO nanoparticles lies in the UV region and therefore UV light source was used for testing of our newly synthesized photocatalyst for the degradation of MB. When ZnO absorbs photon equal to or greater than its bandgap energy, electron could be excited from VB of ZnO to the CB of ZnO and simultaneously leaving a vacancy or "hole" in the VB of ZnO. Generally, these electron–hole pairs recombine quickly, thereby decreasing the photocatalytic activity of bare semiconducting material.[70–72] On modification of ZnO by doping with Nd, the excited electron in the CB can be trapped by Nd, which serves as electron traps and effectively separates the electron hole pair formation. The electrons trapped by Nd would react with oxygen to produce hydroxyl radicals through successive reaction as the final reactive species. Meanwhile, the hole trapped in the VB of Nd-ZnO system would undergo charge transfer to water molecule or hydroxyl group adsorbed on the catalyst surface to generate hydroxyl radicals. The hydroxyl radicals generated during photocatalysis would react with the dye molecules adsorbed on the surface and as a results, the pollutants could be effectively degraded.[73] The above statement is further supported by the previous finding where authors claim that the major species generated in Nd-doped ZnO system is hydroxyl radicals, which are responsible for the degradation of organic pollutants.[40] The formation of hydroxyl radicals in the case of Nd-doped ZnO nanoparticles could be understood by double electron reduction processes as given in eqn (8)–(14).
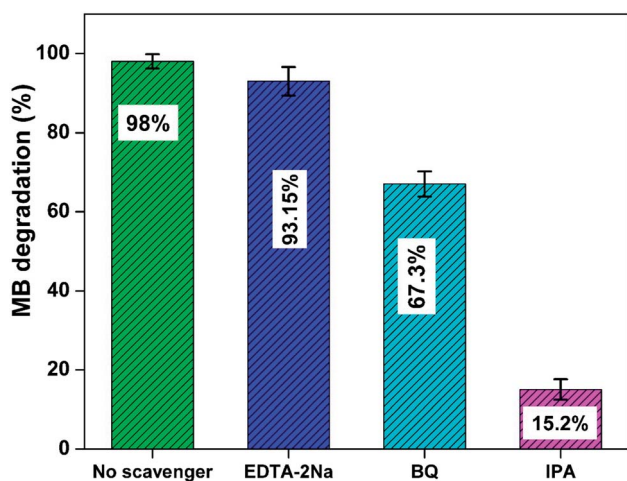
$$ZnO + Nd^{3+} \xrightarrow{h\nu} ZnO\,(h^+) + Nd^{2+} \quad (8)$$

$$Nd^{2+} + O_2 \rightarrow Nd^{3+} + O_2^{•-} \quad (9)$$

$$O_2^{•-} + H^+ \rightarrow HOO^{•} \quad (10)$$

$$HOO^{•} + Nd^{2+} + H^+ \rightarrow H_2O_2 + Nd^{3+} \quad (11)$$

Fig. 10 Degradation percent of MB in the presence of different scavengers over Nd-ZnO; catalyst used 2 g L^{-1}, pH = 10. Error bars showing % error in the three repeated experiments.
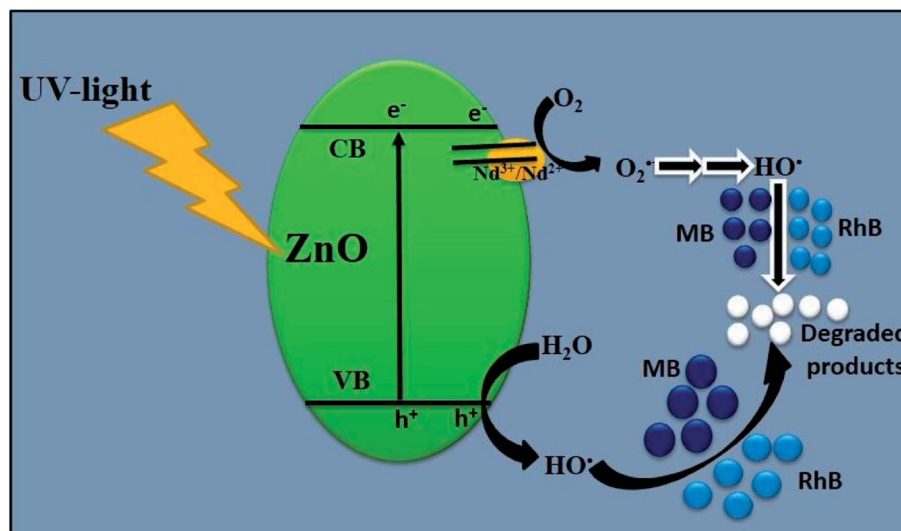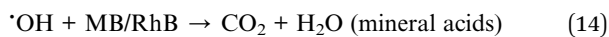
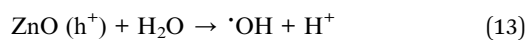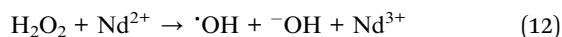**Fig. 12** Schematic illustration of plausible mechanism for the degradation of MB/RhB over Nd-ZnO under UV-light irradiation.

$$H_2O_2 + Nd^{2+} \rightarrow {}^{\bullet}OH + {}^{-}OH + Nd^{3+} \qquad (12)$$

$$ZnO\,(h^+) + H_2O \rightarrow {}^{\bullet}OH + H^+ \qquad (13)$$

$${}^{\bullet}OH + MB/RhB \rightarrow CO_2 + H_2O\ (\text{mineral acids}) \qquad (14)$$

4. Conclusions

In summary, different rare earth metal doped ZnO nanoparticles were prepared by a facile sol–gel route and characterized by different analytical techniques such as XRD, UV-Vis-DRS, SEM-EDS, TEM, BET and TGA analyses. XRD and TEM analyses clearly reveal the hexagonal structure of ZnO nanoparticles which remain unchanged after doping. The slight shift in the diffraction peaks towards lower theta angle and red shift in the absorption spectra clearly indicate the incorporation of rare earth metal into ZnO nanoparticles. The photocatalytic activity of different samples was tested by studying the degradation of MB and RhB under UV-light irradiation. Among the different samples, Nd-doped ZnO nanoparticles was found to be the most active photocatalyst which showed 98% degradation and 68% mineralization of MB during the course of the reaction. The effect of operational parameters such as catalysts loading, reaction pH and effect of oxidants and inorganic ions on degradation of MB was carried out. The results reveal that the optimal degradation conditions for MB degradation are: 2 g L^{-1} catalyst, reaction pH = 10 and 10 ppm MB concentration. Trapping experiments and HO$^{\bullet}$ quantification results imply the involvement of HO$^{\bullet}$ as the main reactive during the photocatalysis process. The mechanism of enhanced photocatalytic activity of Nd-doped ZnO nanoparticles involving charge transfer mechanism through the combined effect of Nd and ZnO has been proposed.

Conflicts of interest

There are no conflicts to declare.

References

1 L.-Y. Yang, S.-Y. Dong, J.-H. Sun, J.-L. Feng, Q.-H. Wu and S.-P. Sun, *J. Hazard. Mater.*, 2010, **179**, 438–443.
2 Z. Han, L. Ren, Z. Cui, C. Chen, H. Pan and J. Chen, *Appl. Catal., B*, 2012, **126**, 298–305.
3 Y. Liu, H. Lv, S. Li, X. Xing and G. Xi, *Dyes Pigm.*, 2012, **95**, 443–449.
4 B. Gao, B. Liu, T. Chen and Q. Yue, *J. Hazard. Mater.*, 2011, **187**, 413–420.
5 A. Szyguła, E. Guibal, M. A. Palacín, M. Ruiz and A. M. Sastre, *J. Environ. Manage.*, 2009, **90**, 2979–2986.
6 F. AlMubaddal, K. AlRumaihi and A. Ajbar, *J. Hazard. Mater.*, 2009, **161**, 431–438.
7 M. G. Méndez-Medrano, E. Kowalska, A. Lehoux, A. Herissan, B. Ohtani, D. Bahena, V. Briois, C. Colbeau-Justin, J. L. Rodríguez-López and H. Remita, *J. Phys. Chem. C*, 2016, **120**, 5143–5154.
8 U. Alam, A. Khan, W. Raza, A. Khan, D. Bahnemann and M. Muneer, *Catal. Today*, 2017, **284**, 169–178.

9 R. Saravanan, M. M. Khan, V. Kumar, E. Mosquera, F. Gracia, V. Narayanan and A. Stephen, *J. Colloid Interface Sci.*, 2015, **452**, 126–133.

10 L. Gnanasekaran, R. Hemamalini, R. Saravanan, K. Ravichandran, F. Gracia, S. Agarwal and V. K. Gupta, *J. Photochem. Photobiol., B*, 2017, **173**, 43–49.

11 H. Li, L. Zhou, L. Wang, Y. Liu, J. Lei and J. Zhang, *Phys. Chem. Chem. Phys.*, 2015, **17**, 17406–17412.

12 A. Khan, U. Alam, W. Raza, D. Bahnemann and M. Muneer, *J. Phys. Chem. Solids*, 2018, **115**, 59–68.

13 W. Fang, M. Xing and J. Zhang, *Appl. Catal., B*, 2014, **160–161**, 240–246.

14 Y. Gu, M. Xing and J. Zhang, *Appl. Surf. Sci.*, 2014, **319**, 8–15.

15 S. Sajjad, S. A. K. Leghari and J. Zhang, *RSC Adv.*, 2013, **3**, 12678–12687.

16 Y. Chen, G. Zhu, M. Hojamberdiev, J. Gao, R. Zhu, C. Wang, X. Wei and P. Liu, *J. Hazard. Mater.*, 2018, **344**, 42–54.

17 S. Bagwas, B. Tian, J. Zhang and M. Nasir, *Chem. Eng. J.*, 2013, **217**, 108–118.

18 U. Alam, M. Fleisch, I. Kretschmer, D. Bahnemann and M. Muneer, *Appl. Catal., B*, 2017, **218**, 758–769.

19 Q. Wang, Q. Ma, J. Lian, J. Zhong, F. Wang, J. Li, Y. He and R. Wang, *New J. Chem.*, 2016, **40**, 5604–5610.

20 D. Qi, M. Xing and J. Zhang, *J. Phys. Chem. C*, 2014, **118**, 7329–7336.

21 R. Saravanan, E. Sacari, F. Gracia, M. M. Khan, E. Mosquera and V. K. Gupta, *J. Mol. Liq.*, 2016, **221**, 1029–1033.

22 X. Shen, B. Tian and J. Zhang, *Catal. Today*, 2013, **201**, 151–158.

23 M. Samadi, M. Zirak, A. Naseri, E. Khorashadizade and A. Z. Moshfegh, *Thin Solid Films*, 2016, **605**, 2–19.

24 P. Zhang, P. Wu, S. Bao, Z. Wang, B. Tian and J. Zhang, *Chem. Eng. J.*, 2016, **306**, 1151–1161.

25 S. Lan, L. Liu, R. Li, Z. Leng and S. Gan, *Ind. Eng. Chem. Res.*, 2014, **53**, 3131–3139.

26 R. Shao, L. Sun, L. Tang and Z. Chen, *Chem. Eng. J.*, 2013, **217**, 185–191.

27 M. Misra, P. Kapur and M. L. Singla, *Appl. Catal., B*, 2014, **150–151**, 605–611.

28 P. Pawinrat, O. Mekasuwandumrong and J. Panpranot, *Catal. Commun.*, 2009, **10**, 1380–1385.

29 S. G. Kumar and K. S. R. K. Rao, *RSC Adv.*, 2015, **5**, 3306–3351.

30 C. Han, M.-Q. Yang, B. Weng and Y.-J. Xu, *Phys. Chem. Chem. Phys.*, 2014, **16**, 16891–16903.

31 V. Vaiano, M. Matarangolo, O. Sacco and D. Sannino, *Appl. Catal., B*, 2017, **209**, 621–630.

32 G. Cappelletti, V. Pifferi, S. Mostoni, L. Falciola, C. D. Bari, F. Spadavecchia, D. Meroni, E. Davoli, S. Ardizzone, S. Morandi and E. Davoli, *Chem. Commun.*, 2015, **51**, 10459–10462.

33 Ş. Ş. Türkyılmaz, N. Güy and M. Özacar, *J. Photochem. Photobiol., A*, 2017, **341**, 39–50.

34 N. C. S. Selvam, J. J. Vijaya and L. J. Kennedy, *J. Colloid Interface Sci.*, 2013, **407**, 215–224.

35 A. N. Ökte, *Appl. Catal., A*, 2014, **475**, 27–39.

36 M. Khatamian, A. A. Khandar, B. Divband, M. Haghighi and S. Ebrahimiasl, *J. Mol. Catal. A: Chem.*, 2012, **365**, 120–127.

37 M. Myilsamy, M. Mahalakshmi, N. Subha, A. Rajabhuvaneswari, V. Murugesan, H. Sakurai, T. Kobayashi, S. H. Hur, Z. Zeng, J. Zhang, I. A. Aksay and J. Liu, *RSC Adv.*, 2016, **6**, 35024–35035.

38 A. Sarkar, A. B. Ghosh, N. Saha, A. K. Dutta, D. N. Srivastava, P. Paul, B. Adhikary, K. Fujita, K. Tanaka, T. Kawaj and H. Kominami, *Catal. Sci. Technol.*, 2015, **5**, 4055–4063.

39 K. T. Ranjit, I. Willner, S. H. Bossmann and A. M. Braun, *Environ. Sci. Technol.*, 2001, **35**, 1544–1549.

40 J.-C. Sin, S.-M. Lam, K.-T. Lee and A. R. Mohamed, *Ceram. Int.*, 2014, **40**, 5431–5440.

41 B. Roy, S. Chakrabarty, O. Mondal, M. Pal and A. Dutta, *Mater. Charact.*, 2012, **70**, 1–7.

42 S. Anandan, A. Vinu, K. L. P. Sheeja Lovely, N. Gokulakrishnan, P. Srinivasu, T. Mori, V. Murugesan, V. Sivamurugan and K. Ariga, *J. Mol. Catal. A: Chem.*, 2007, **266**, 149–157.

43 W. Chen, J.-O. Bovin, A. G. Joly, S. Wang, F. Su and G. Li, *J. Phys. Chem. B*, 2004, **108**, 11927–11934.

44 L. Zhang, Y. Yang, R. Fan, J. Yu and L. Li, *J. Mater. Chem. A*, 2013, **1**, 12066–12073.

45 V. Štengl, S. Bakardjieva and N. Murafa, *Mater. Chem. Phys.*, 2009, **114**, 217–226.

46 Y. Guo, G. Zhang, H. Gan and Y. Zhang, *Dalton Trans.*, 2012, **41**, 12697–12703.

47 A. K. L. Sajjad, S. Shamaila, B. Tian, F. Chen and J. Zhang, *Appl. Catal., B*, 2009, **91**, 397–405.

48 Q.-P. Luo, X.-Y. Yu, B.-X. Lei, H.-Y. Chen, D.-B. Kuang and C.-Y. Su, *J. Phys. Chem. C*, 2012, **116**, 8111–8117.

49 Y. Zhang, L. Deng, G. Zhang and H. Gan, *Colloids Surf., A*, 2011, **384**, 137–144.

50 Y. Guo, G. Zhang, J. Liu and Y. Zhang, *RSC Adv.*, 2013, **3**, 2963–2970.

51 B. Subash, B. Krishnakumar, M. Swaminathan and M. Shanthi, *Mater. Sci. Semicond. Process.*, 2013, **16**, 1070–1078.

52 B. Subash, B. Krishnakumar, R. Velmurugan, M. Swaminathan and M. Shanthi, *Catal. Sci. Technol.*, 2012, **2**, 2319–2326.

53 Y. Zhang, D. Wang and G. Zhang, *Chem. Eng. J.*, 2011, **173**, 1–10.

54 Y. Zhang, H. Gan and G. Zhang, *Chem. Eng. J.*, 2011, **172**, 936–943.

55 S. Kansal, N. Kaur and S. Singh, *Nanoscale Res. Lett.*, 2009, **4**, 709–716.

56 B. Krishnakumar and T. Imae, *Appl. Catal., A*, 2014, **486**, 170–175.

57 B. Krishnakumar and M. Swaminathan, *Spectrochim. Acta, Part A*, 2012, **99**, 160–165.

58 K. Vignesh, M. Rajarajan and A. Suganthi, *J. Ind. Eng. Chem.*, 2014, **20**, 3826–3833.

59 S. Harish, M. Navaneethan, J. Archana, A. Silambarasan, S. Ponnusamy, C. Muthamizhchelvan and Y. Hayakawa, *Dalton Trans.*, 2015, **44**, 10490–10498.

60 R. Nagaraja, N. Kottam, C. R. Girija and B. M. Nagabhushana, *Powder Technol.*, 2012, **215–216**, 91–97.

61 P. Velusamy and G. Lakshmi, *Appl. Water Sci.*, 2017, **7**, 4025–4036.

62 B. Krishnakumar, B. Subash and M. Swaminathan, *Sep. Purif. Technol.*, 2012, **85**, 35–44.

63 B. Krishnakumar, K. Selvam, R. Velmurugan and M. Swaminathan, *Desalin. Water Treat.*, 2010, **24**, 132–139.

64 M. Muneer and D. Bahnemann, *Appl. Catal., B*, 2002, **36**, 95–111.

65 N. Sobana and M. Swaminathan, *Sep. Purif. Technol.*, 2007, **56**, 101–107.

66 G. Thennarasu and A. Sivasamy, *Powder Technol.*, 2013, **250**, 1–12.

67 A. Khataee, R. D. C. Soltani, Y. Hanifehpour, M. Safarpour, H. G. Ranjbar and S. W. Joo, *Ind. Eng. Chem. Res.*, 2014, **53**, 1924–1932.

68 T. Liu, G. Tan, C. Zhao, C. Xu, Y. Su, Y. Wang, H. Ren, A. Xia, D. Shao and S. Yan, *Appl. Catal., B*, 2017, **213**, 87–96.

69 U. Alam, S. Kumar, D. Bahnemann, J. Koch, C. Tegenkamp and M. Muneer, *Phys. Chem. Chem. Phys.*, 2018, **20**, 4538–4545.

70 G. Dong, Z. Ai and L. Zhang, *RSC Adv.*, 2014, **4**, 5553–5560.

71 G. Dong and L. Zhang, *J. Mater. Chem.*, 2012, **22**, 1160–1166.

72 J. Jiang, L. Zhang, H. Li, W. Hec and J. J. Yin, *Nanoscale*, 2013, **5**, 10573–10581.

73 U. Alam, A. Khan, D. Bahnemann and M. Muneer, *J. Colloid Interface Sci.*, 2018, **509**, 68–72.